Reprinted from MONTHLY WEATHER REVIEW, Vol. 121, No. 10, October 1993
American Meteorological Society

An Introduction to Wavelet Analysis in Oceanography and Meteorology: With Application to the Dispersion of Yanai Waves

S. D. MEYERS, B. G. KELLY, AND J. J. O'BRIEN

An Introduction to Wavelet Analysis in Oceanography and Meteorology: With Application to the Dispersion of Yanai Waves

S. D. MEYERS, B. G. KELLY, AND J. J. O'BRIEN

Mesoscale Air–Sea Interaction Group, The Florida State University, Tallahassee, Florida

(Manuscript received 30 October 1992, in final form 4 May 1993)

ABSTRACT

Wavelet analysis is a relatively new technique that is an important addition to standard signal analysis methods. Unlike Fourier analysis that yields an average amplitude and phase for each harmonic in a dataset, the wavelet transform produces an "instantaneous" estimate or local value for the amplitude and phase of each harmonic. This allows detailed study of nonstationary spatial or time-dependent signal characteristics.

The wavelet transform is discussed, examples are given, and some methods for preprocessing data for wavelet analysis are compared. By studying the dispersion of Yanai waves in a reduced gravity equatorial model, the usefulness of the transform is demonstrated. The group velocity is measured directly over a finite range of wavenumbers by examining the time evolution of the transform. The results agree well with linear theory at higher wavenumber but the measured group velocity is reduced at lower wavenumbers, possibly due to interaction with the basin boundaries.

1. Introduction

a. The wavelet transform

The wavelet transform has shown promise in a diversity of scientific fields, but to date it has not been much used in the oceanic and atmospheric sciences. In part, this might be due to a lack of material discussing practical aspects of the technique. This article therefore includes an introduction to the wavelet transform as a tool for data analysis. For brevity, we shall confine our discussion to the transform of a scalar series $f(t)$.

Wavelet analysis is based on the convolution of $f(t)$ with a set of functions $g_{ab}(t)$ derived from the translations and dilations (and rotations in higher dimensions) of a *mother wavelet* $g(t)$, where

$$g_{ab}(t) = \frac{g}{a^{1/2}}\left(\frac{t-b}{a}\right); \qquad (1)$$

$a(>0)$ and b are real. Any set of functions $g_{ab}(t)$ constructed from (1) and meeting the conditions outlined below are called *wavelets*. The convolution of $f(t)$ with the set of wavelets is the *wavelet transform* (WT)

$$T_g(b, a) = \frac{1}{a^{1/2}}\int g\left(\frac{t-b}{a}\right) f(t)dt. \qquad (2)$$

Corresponding author address: Dr. Steven D. Meyers, Mesoscale Air–Sea Interaction Group, The Florida State University, B-174, 020 Love Building, Tallahassee, FL 32306-3041.

This is known as the continuous wavelet transform since a and b may be varied continuously. Translation parameter b corresponds to position or time if the data is spatial or temporal, respectively. Dilation parameter a then corresponds to scale length or temporal period. Equation (2) expands a one-dimensional time series into the two-dimensional parameter space (b, a) and yields a local measure of the relative amplitude of activity at scale a at time b. This is in contrast to the Fourier transform that yields an average amplitude over the entire dataset. Note, we have avoided the use of the words "wavelength" or "frequency" in our description of the WT. Though wavelets have a definite scale, they need not bear any resemblance to Fourier modes (sines and cosines). However, a correspondence between wavelength and scale a sometimes can be achieved, as discussed in section 3.

To see the limitation of standard Fourier analysis and the incentive for the development of wavelet analysis, consider the time series in Fig. 1a that changes frequency halfway through the measurement. Compare that to the signal in Fig. 1b that is generated from the simultaneous presence of both frequencies. These two very different signals yield similar power spectra, shown in Figs. 1c,d, both being dominated by the same two peaks. Without prior knowledge, it would be difficult to know which signal produced which spectrum, since information on signal evolution is lost during Fourier analysis. Variations of the Fourier transform have been used (e.g., Gabor 1946) in attempts to overcome this limitation, but have met only with qualified success. The WT produces "instantaneous" coefficients and

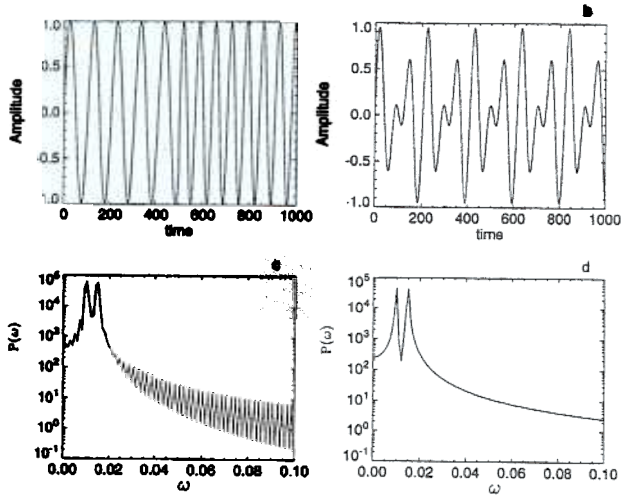

FIG. 1. A limitation of standard Fourier analysis is illustrated; very different signals can have very similar power spectra: (a) a monochromatic signal that changes frequency halfway through the dataset, (b) a signal comprised of two frequencies, (c) the raw power spectrum of (a), and (d) the raw power spectrum of (b).

therefore can yield information on the evolution of nonstationary processes.

The development of wavelet analysis began relatively recently with Morlet (1983). A later collaboration (Grossman and Morlet 1984) produced the continuous wavelet transform in one dimension based on the set of translations and dilations. Meyer (1985) extended the technique to n dimensions, and Murenzi (1989) included rotation. Three references are used for the introduction to wavelet analysis: Farge (1992), Ruskai et al. (1992), and Combes et al. (1989). Our goal in this article is not to give a complete review of the wavelet transform but to aid in its introduction to oceanographers and meteorologists. The references contain details on the history and uses of wavelets in a variety of scientific applications.

In the following we continue with the introduction to wavelet analysis. In section 2, a few methods for preprocessing data for wavelet analysis are discussed. Two simple methods from Fourier analysis are tried and shown to be inappropriate as they distort the end regions of the WT. Another method, based on buffering the ends of the data with additional points, is shown to yield better results. Section 3 examines the dispersion of Yanai waves and demonstrates how quantitative information not available from Fourier methods can be obtained using the WT.

b. *Wavelet selection*

To be a mother wavelet both formally and in practice, $g(t)$ must have the following properties.

(i) It must be a function centered at zero and in the limit as $|t| \to \infty$, $g(t) \to 0$ rapidly. This condition produces the local nature of wavelet analysis, since the coefficients $T_g(b, a)$ are affected only by the signal in the *cone of influence* (COI) about $t = b$. In practice, the radius of the COI is the point $|t| = r_c$ beyond which $g_{ab}(x)$ no longer has significant value. Usually, $r_c \propto a$, giving rise to conelike structures in the WT in certain cases. The COI of the endpoints is an important consideration and will be discussed further in section 2.

(ii) Also, $g(t)$ must have zero mean. Known as the admissibility condition, this implies the invertability of the WT. That is, the original signal can be obtained from the wavelet coefficients using

$$f(t) = \frac{1}{C}\int\int \frac{T_g(b, a)g_{ab}}{a^2}\, dadb$$

where

$$\frac{1}{C} = \int_{\infty}^{\infty} \frac{|\hat{g}(\omega)|^2}{\omega}\, d\omega .$$

The caret indicates Fourier transform. For C^{-1} to remain finite, $\hat{g}(0)$ must equal zero.

(iii) Wavelets are often regular; that is, $\hat{g}(\omega < 0) = 0$. This simplifies the interpretation of the transform because it eliminates confusion of measurements at ω with those at $-\omega$. Wavelets that are regular are also called *progressive.*

(iv) Higher-order moments should vanish, allowing for the study of high-order variations in the data. This requirement can be relaxed, depending on the application.

The quantitative result of a WT depends upon the form of $g(t)$. A clear example is the choice of complex versus real wavelets. Complex wavelets allow the separation of the magnitude and phase of the data, whereas real wavelets, loosely speaking, superpose both measurements in the (b, a) plane. The complex transform is more easily interpreted and is the type of wavelet used in this article. Some examples of mother wavelets were shown in Farge (1992) and Coulibaly (1992), for example. However, they represented only a few cases from an infinite family of functions; many other wavelets are known or are under study.

The appropriate choice of $g(t)$ is dictated by the goals of the analysis. Suppose one is seeking the simultaneous presence of two frequencies, c_1 and c_2, within a signal. An appropriate mother wavelet is

$$g(t) = (e^{ic_1t}e^{ic_2t})e^{-t^2/2}. \tag{3}$$

If one is seeking "chirps" (short segments of linearly increasing frequency), the wavelet

$$g(t) = e^{ikt^2/2}e^{ict}e^{-t^2/2} \tag{4}$$

would be useful. If one knows the characteristics of the signal or pattern being sought, the wavelet should be chosen to have that same pattern. Large values of

$|T_g(b, a)|$ will then indicate where $f(t)$ has the desired form.

Not only are there trade-offs in choosing $g(t)$ but there are considerations when choosing a and b. For example, the continuous wavelet transform can yield redundant information since small changes in a or b are often insignificant. A more efficient choice is to choose a discrete set of a and b such that the $g_{ab}(t)$ constitute an orthogonal basis set. The WT at any parameter value can then be found using a suitable interpolation scheme. There is much discussion of these discrete wavelets in the literature, as they are useful in fields such as image compression and multiresolution analysis.

c. *Wavelet algorithms*

There are several algorithms to implement a WT, and only two will be discussed here. The references detail other methods under development, particularly those involving discrete wavelets. Here, we discuss the continuous transform.

The simplest method is direct numerical integration. Knowing $f(t)$ and $g(t)$, one can compute the transform at arbitrary points in parameter space using a discretized form of (2). The drawback of this technique is that it is time consuming. If one integrates over $0 < a \leq I$ and $0 < b \leq J$, the integration time goes as IJ^2.

An alternative is to exploit the convolution theorem and do the WT in spectral space:

$$T_b(b, a) = a^{1/2} \int e^{ib\omega} \hat{g}^*(a\omega) \hat{f}(\omega) d\omega. \quad (5)$$

This allows the use of optimized fast Fourier transform (FFT) routines and results in a much faster transform, with CPU time going as $IJ \log_2 J$. To use this method, $\hat{g}(\omega)$ should be known analytically and the data must be preprocessed to avoid errors from the FFT algorithms. In particular, the discrete form of (5) will produce an artificial periodicity in the WT if $f(t)$ is not periodic. This is demonstrated in the examples herein, and different methods for dealing with the problem are discussed. Issues of aliasing and bias in FFT routines are well known and need not be discussed here.

2. Examples of wavelet analysis

The WT of the signal in Fig. 1a is a classic example in wavelet literature and will be examined with four different data preparation methods. All follow (5) and use the Morlet wavelet $g(t) = e^{ict}e^{-t^2/2}$. Method I does not involve any preparation of the data, and the transform is computed without considering the properties of FFT routines. The result is presented in Fig. 2, with the amplitude and phase shown separately. As in all the transforms shown here, the vertical axis is the inverted scale a, so the corresponding wavenumber increases on the vertical axis. The horizontal axis is time b. The mesh in all the plates indicates the COI of the endpoints. Consider the first endpoint $t = 0$. For $b < r_c$, the wavelet has significant values at $t < 0$ where there is no signal. Hence, there is a steady degradation in the WT as b approaches 0.

Regions where $|T_g(b, a)|$ are large indicate high correlation between the data and the wavelet. In Fig. 2, the modulus clearly indicates the abrupt change in the frequency of the signal by the shift of the large coefficients to a different scale. The phase indicates the cycling of the signal from $-\pi$ to π and allows for the location of wave crests in the signal. One can count the number of waves in a simple signal such as the one shown here. The branchings at larger a are due to the larger wavelets (large a) detecting more than one cycle. Note the convergence of the phase lines toward higher frequency (smaller a) in the middle of the transform. This indicates when the frequency shifted, and generally occurs at any singularity (sudden changes in frequency or phase) in the signal. Interpretation of phase plots for more complicated signals can be nontrivial.

In the WT phase, and to a lesser extent in the modulus, activity is indicated at many scales, though the signal is locally monochromatic. Although there is a "best" choice for the scale ($a = a_0$) in the modulus, the nonzero correlations between the wavelets and data produce nonzero transform values at scales away from a_0. This can lead to confusion when trying to determine which scales are present in the data; one method for dealing with this problem is discussed in the next section.

Note in Fig. 2 the curvature of the modulus at the end regions. The line of maximum wavelet coefficient bends to meet artificial periodic boundary conditions, falsely indicating frequency changes at the beginning and end of the signal. This demonstrates the generic problem when using (5) on nonperiodic data—the WT can induce a periodicity into the transform, greatly distorting the information at the end regions. This is a critical problem when the initial and final signal characteristics are very different.

In an attempt to impose periodicity on the signal, method II preprocesses $f(t)$ with a cosine window

$$f(t_k) \rightarrow f(t_k)\left[1 - \cos^2\left(\frac{k\pi}{N-}\right)\right]$$

$$k = 0, 1, \cdots, (N-1); \quad (6)$$

N is the total number of data points. The resulting WT no longer has the false end regions, because it has effectively lost those areas, as seen in Fig. 3, which is clearly an unacceptable effect. A window with steep cutoffs would not eliminate as much data but would produce only a small correction to the distortion of the end regions.

Method III involves detrending $f(t_k)$ and removing the mean, a standard procedure when computing FFTs.

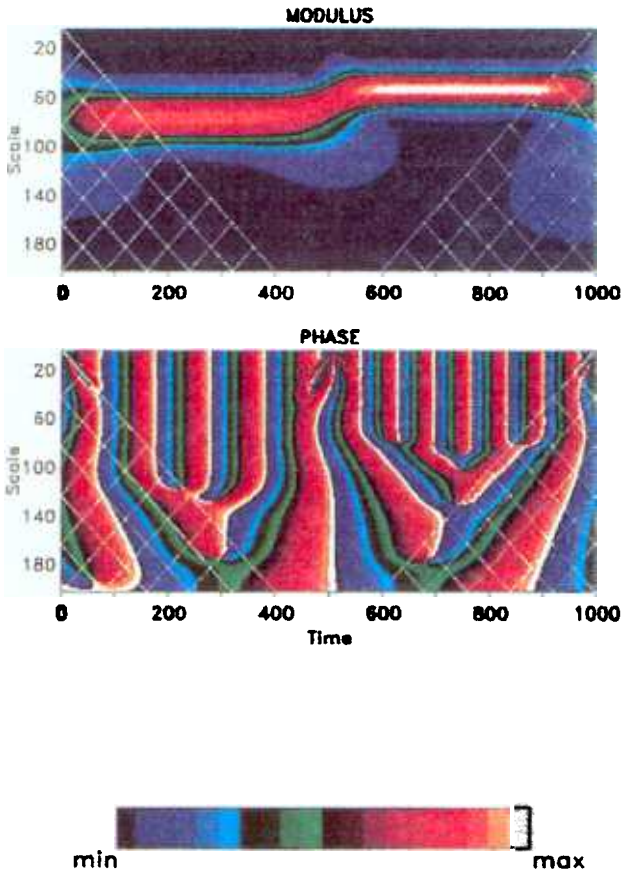

FIG. 2. Wavelet transform of the signal in Fig. 1a using $f(t)$ that was not preconditioned. The change in frequency is clearly indicated by the shift in the wavelet modulus maximum. False results are produced at the end regions since the data is not periodic. (a) Modulus: the colors represent values from the minimum (blue) to the maximum (white). (b) Phase: the colors represent values from $-\pi$ (blue) to π (white). The vertical axis is the inverted a scale. The mesh indicates the COI ($r_c = 2a$ for the Morlet wavelet). The color bar is used in this figure and Fig. 8 with the minimum and maximum adjusted for each plot.

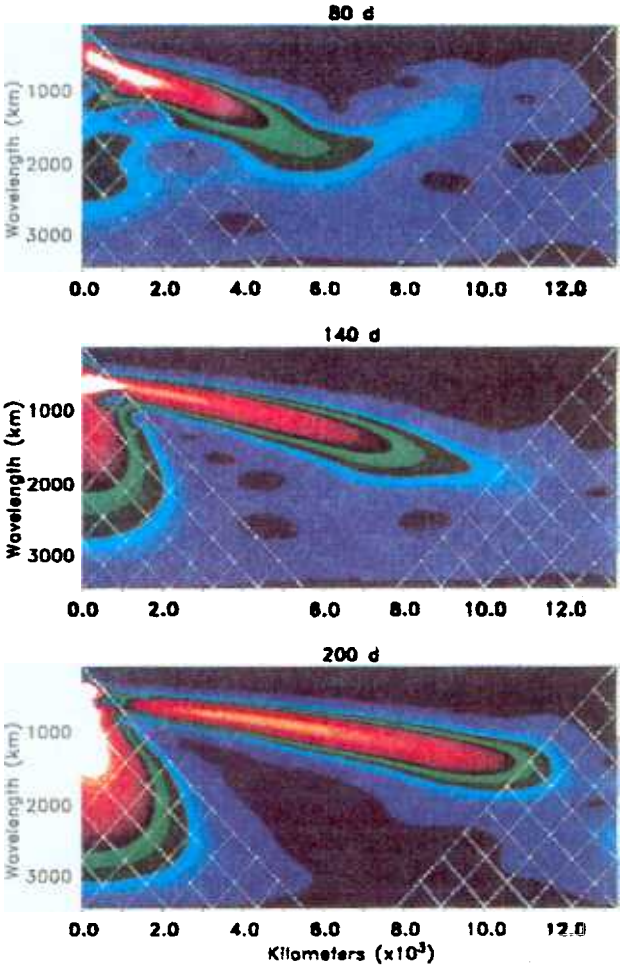

FIG. 8. The modulus of the WT of the height fields in Fig. 7. Vertical axis is the wavelength λ given by Eq. (12), and the horizontal axis is distance across the model basin. Note the progression of the tongue from the upper left toward the lower right in time, corresponding to the changes in wavelength as the Yanai waves disperse across the basin: (a) 80, (b) 140, and (c) 200 days. White is the maximum coefficient, and blue is the minimum. The radius of the COI mesh is $r_c = 2\lambda/1.2$.

The result is shown in Fig. 4. Again, errors in the wavelet coefficients appear as they did with method I. Though methods II and III are common methods for preparing data for Fourier analysis, they are inadequate for wavelet analysis.

Method IV, though developed independently by the authors, has already been investigated by other researchers (Barnier 1992, personal communication). The data $f(t_k)$ is buffered on either side with a tail that goes to zero, as indicated in Fig. 5. After the WT is complete, the regions corresponding to the tails are discarded, yielding Fig. 6. This method eliminates the problem of nonperiodic data and does not introduce significant distortions of the end regions. The length of the buffers are chosen empirically. When the buffers are too short, distortions as in Fig. 2 are found but lessen as the buffer length is increased. Various forms of the buffers can be chosen. Here, we used a very simple form, but suggest for future applications matching not just the endpoint values but their derivatives as well. Even better would be a form that matches the endpoint frequency, amplitude, and phase, which is conceivable for simple signals, and would arguably eliminate most of the problems associated with the COI at the endpoints. Of course, if the end regions are unimportant, their WT can be ignored.

A frequent comment about wavelet analysis is that it is difficult to obtain more than qualitative information (such as detecting the frequency change in the preceding example). This may be so in some cases; in others it is possible to obtain quantitative information that would be difficult if not impossible to obtain by

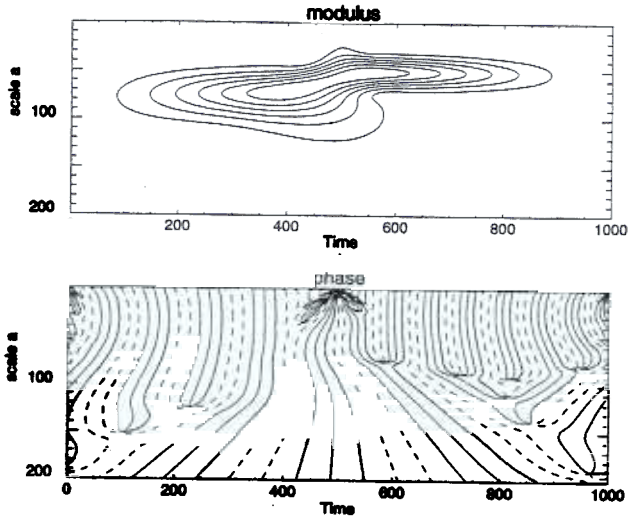

FIG. 3. Contours of the wavelet transform of the signal in Fig. 1a using $f(t)$ that was preconditioned using a cosine window. The information in the end regions is now lost: (a) modulus; (b) phase. The negative contours are dashed.

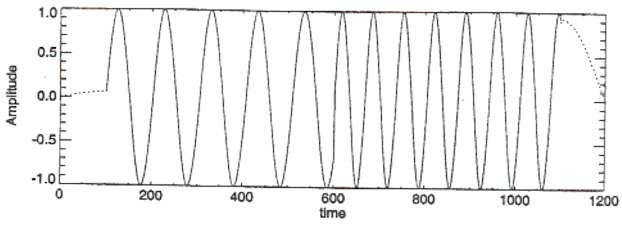

FIG. 5. Buffering of the signal in Fig. 1a. The data is made periodic by adding tails to the end points of $f(t)$. The original data is indicated by the solid line, and the additional buffering with dotted lines. The regions corresponding to the buffers are discarded after WT.

traditional Fourier analysis. As a practical illustration of wavelet analysis we will directly measure the dispersion of Yanai waves in an ocean model. The results indicate general agreement with linear theory except near the eastern boundary where the wave propagation appears to slow. The spectral ocean model used to create the data is described by Kelly (1992).

3. Dispersion of Yanai waves

Instability waves in the equatorial regions of the world's oceans have been under study since the mid-1970s. Interest began following the observations made during the GARP (Global Atmospheric Research Project) Atlantic Tropical Experiment (GATE) in the summer of 1974 (Duing et al. 1975). Occurring in a narrow frequency band, with periods around 25 days and zonal wavelengths of about 1000 km, their structure has been shown to be dynamically similar to Yanai waves (mixed Rossby–gravity waves) both in the observations (Weisberg and Horigan 1981; Tsai 1990) and in the numerical models (Cox 1980; Kindle and Thompson 1989; Woodberry et al. 1989). The waves propagate westward and upward with a group velocity that is eastward and downward (Weisberg et al. 1979; Cox 1980). The zonal phase and group velocities are about 33–73 cm s^{-1} and 16 cm s^{-1}, respectively (Weisberg et al. 1979). Similar oscillations were observed along the equatorial front in the eastern tropical Pacific using satellite imagery (Legeckis 1977).

As a result of these observations, it was hypothesized that they were generated by a meridional shear instability between the westward-flowing South Equatorial Current (SEC) and the eastward-flowing North Equa-

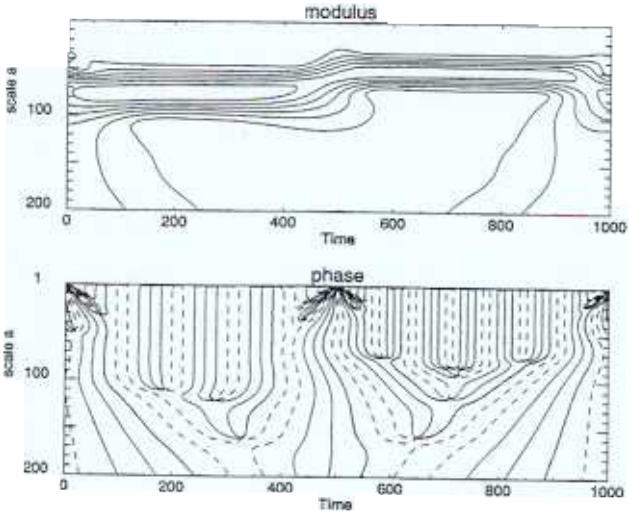

FIG. 4. Wavelet transform of the signal in Fig. 1a using $f(t)$ that was demeaned and detrended; (a) and (b) as in Fig. 3.

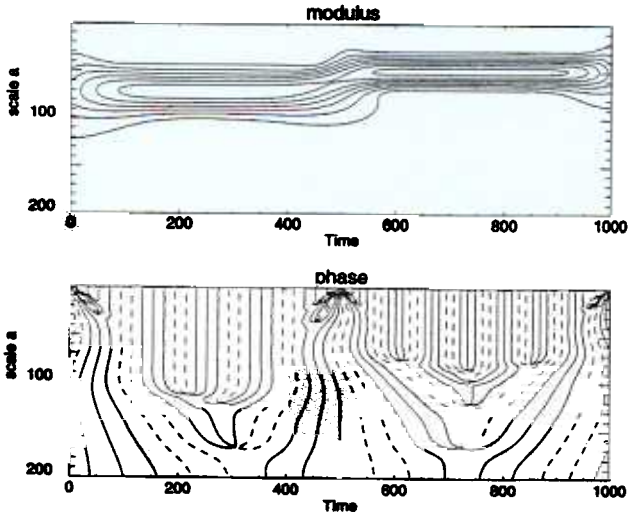

FIG. 6. Wavelet transform of the signal in Fig. 5. There is much less distortion in the end regions of the data. Buffer length was 100 data points.

torial Countercurrent (NECC) (Philander 1976, 1978). A more recent study by Weisberg and Weingartner (1988) showed that the generation region of the waves is slightly to the south of the boundary between the SEC and the NECC. Nevertheless, there is a general agreement that for the eastern tropical Atlantic and Pacific the waves are caused by a latitudinal shear instability. A different mechanism has been proposed for the western Indian Ocean where the waves are more likely to be boundary forced (Kindle and Thompson 1989; Woodberry et al. 1989; Moore and McCreary 1990). A hypothesis that the waves in this region result from cross-equatorial wind stress has been presented, with the preferred frequency selection around 25 days being due to the dispersive properties of Yanai waves (Kelly 1992). We now discuss how the wavelet transform was useful in supporting this idea.

The linear dispersion relation for Yanai waves (Moore and Philander 1977) is

$$k = \frac{\sigma}{c} - \frac{\beta}{\sigma}, \qquad (7)$$

where k is the wavenumber, σ is the frequency, and $c = (g'H)^{1/2}$. From (7), Yanai waves with westward phase speed have eastward group velocity with c_g increasing as $k \to 0^-$ so the longer waves propagate faster. This is reflected in the pattern of the measured antisymmetric height field

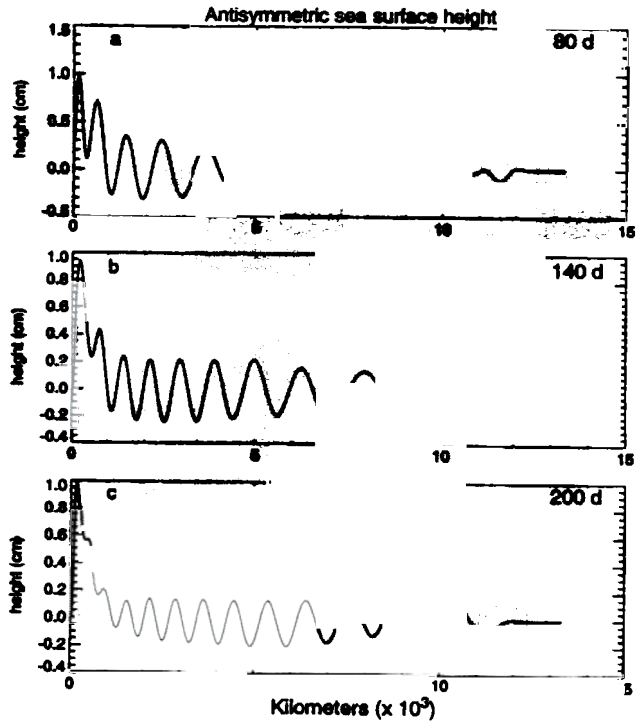

FIG. 7. Cross-longitudinal sections at three different days of the height field along 3°N. Note the change in wavelength with longitude: (a) 80, (b) 140, and (c) 200 days.

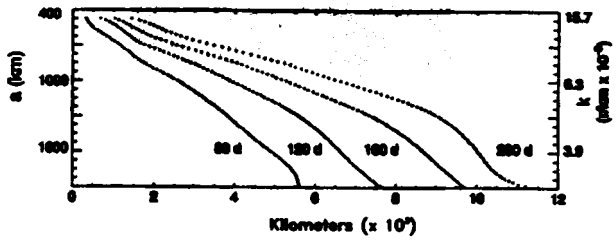

FIG. 9. The transform maximums corresponding to the dispersion tongues. The evolution of the line in time gives the group velocity. Note the gradual flattening of the lines in the western region.

$$h_A(x, y) = \frac{1}{2}[h(x, y) - h(x, -y)], \qquad (8)$$

which shows a wavelength increasing eastward across the basin. Since the $h(x, y)$ field for a Yanai wave is antisymmetric about the equator, measurements of h_A help isolate the relatively small-amplitude Yanai waves from the large-amplitude symmetric structures (e.g., Kelvin waves). Cross-longitudinal measurements of $h_A(x, y = +3°)$ are shown for 80, 140, and 200 model days in Fig. 7. It is clear that wavenumber depends on longitude and that the waves are propagating energy eastward. A similar wave pattern was found in a reduced gravity model by Kindle and Thompson (1989). Though power spectra would indicate which wavenumbers are present, no understanding of the spatial characteristics could be achieved.

In contrast, the WTs clearly show the structure of the wave field and its development in time. Figure 8 (see p. 2861) shows the modulus of the transform at 80, 140, and 200 days, which indicates the waves as a tongue of high values stretching progressively farther across the basin. The vertical coordinate is the Fourier mode that corresponds to wavelet scale (Appendix).

To obtain quantitative results from the transforms, the modulus is scanned along each scale for local maximum, revealing the "spine" of the dispersion tongue. (The result of a scan over the entire transform is sometimes called a "skeleton.") Since it is at these local maximum that the maximum correlation of the wavelet and $f(t)$ occurs, we assume it is the motion of the maximum points that best indicate the dynamics. The points in Fig. 9 are the maximum points corresponding to the dispersive tongues in the modulus of several WTs. Using these results, we can now directly obtain the range of scales involved and the distance that they have propagated. Measuring the displacement of the spine at each scale over time yields the group speed $c_g(a)$. Note in Fig. 9 that the total displacement of the lines is greater at the smaller wavenumbers, indicating larger group velocity.

The relation between the wavenumber k of the Fourier modes and the scale a is not fully understood and may not be useful with irregular wavelets. However, in the case of the Morlet wavelet a relation can be obtained by transforming a monochromatic signal as dis-

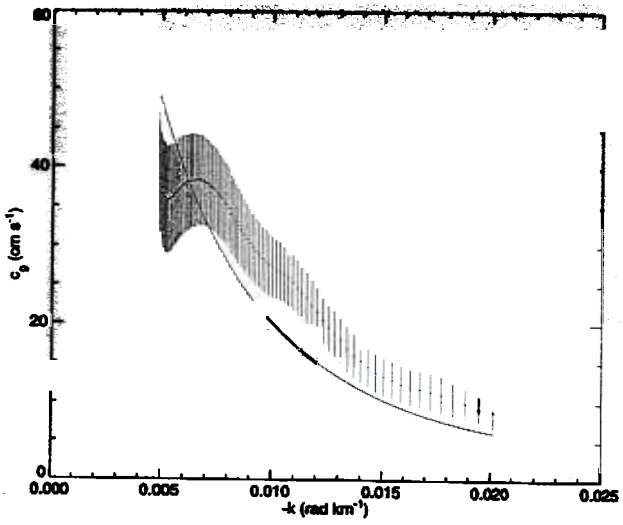

FIG. 10. The measured dispersion relation from the WT. Error bars are based on the standard deviation of the measured velocity. The theoretical value is shown as the solid curve. Wavenumbers are assumed to be $k = 2.1(2\pi)a^{-1}$.

cussed in the Appendix. Such a transform would have a structure as in Fig. 6 but with a single maximum of the modulus in a. The line of maximum correlation yields a conversion from wavelet scale to Fourier wavelength. For the Morlet wavelet with $c = 5$ (used in the WT in this article), the wavelength is given by $\lambda \approx 1.2a$. This allows us to compare the measurements of propagation speed with the theoretical speed at conventional wavenumbers.

The results of the measured c_g are compared with theoretical values in Fig. 10. There is general agreement with the linear theory in the range from approximately $k = -0.005$ rad km^{-1} to $k = -0.02$ rad km^{-1}. (Note, we deal only with $k < 0$.) For smaller k the measured c_g diverges from the theoretical value, possibly due to the finite size of the basin. When the maxima for all the days under study are plotted together, one can see a sudden decrease in the propagation speed of wavelengths above 1600 km when they near the eastern boundary. This scale corresponds to the value of k where the drop-off in c_g occurs. To test this we expanded the basin domain from 15 000 to 22 500 km, while keeping the same number of modes in the spectral model. In the longer domain there is no drop-off of the measured group velocity at lower wavenumber since the longer waves do not have time to encounter the eastern boundary during 200 model days.

As mentioned in Kelly (1992), in the western region of the basin Yanai waves exist only in a limited range of k. Examining Fig. 9, one can see a gradual flattening of the curves in the western basin as time progresses, indicating a narrowing of the range of wavenumbers. The waves remaining in the west are several hundred kilometers in wavelength, as observed in the Indian Ocean. This suggests that the narrow range of periods found in the ocean may be due to the dispersion of Yanai waves; the longer, faster waves leave the western region after roughly 100 days.

4. Summary

The wavelet transform promises to be a useful tool in oceanography and meteorology. For the purpose of data analysis, the continuous transform in spectral space is useful and efficient. However, standard methods for preprocessing data for Fourier analysis are insufficient for wavelet analysis. The best method examined here is that of buffering the ends of the signal with points that smoothly go to zero. The region of the transform corresponding to these points is then discarded after the transform. Without this buffering, a signal whose properties are different near its ends will result in a WT that has been forced to periodicity at all scales through a distortion (in some cases severe) of the end regions. The greater the aperiodicity of the signal, the greater the distortion.

We demonstrate the usefulness of the WT by examining the dispersion of Yanai waves. The transform modulus clearly reveals the propagation of the different wavelengths across the basin. By scanning the modulus, $c_g(k)$ is measured directly and shown to agree with linear theory, though there is a reduction in propagation speed of the longer wavelengths. The narrowing of the range of wavelengths in the western region observed supports the hypothesis that the narrow range of frequencies observed in the western equatorial oceans is a consequence of Yanai wave dispersion. These results could not be obtained using standard Fourier techniques.

The use of wavelets goes beyond simple data analysis, and a full discussion is beyond the scope of the paper, but a couple of references might suggest possible future applications. An extension of wavelet analysis, called *multiresolution analysis*, adds the *scaling functions* $\phi(x)$ to the set of wavelets, where in contrast to condition (i) in section 1,

$$\int_{-\infty}^{\infty} \phi(x)dx = 1.$$

The addition of the scaling functions to the set of wavelets allows for the decomposition of functions that are not square integrable.

Frequently used with discrete wavelets [following the notation of Farge (1992)] $\psi_{ij}(x)$ that are defined by $\psi_{ij}(x) = 2^{j/2}\psi(2^j x - i)$, the reconstruction equation for $f(x)$ is then

$$f(x) = \sum_{i=-\infty}^{+\infty} \langle \phi_{0i} | f(x) \rangle \phi_{0i}(x) + \sum_{j=0}^{+\infty} \sum_{i=-\infty}^{+\infty} \langle \psi_{ij} | f(x) \rangle \psi_{ij}(x) \quad (9)$$

Of more direct interest to the reader might be recent attempts to model two- and three-dimensional fluids in wavelet space. A representation of the three-dimensional Navier–Stokes equation in wavelet space is given by Meneveau (1991), with the emphasis on reducing the number of degrees of freedom necessary for modeling fluid turbulence. Zimin (1981), antecedent to the formal development of wavelets, studied the Navier–Stokes equation in terms of basis functions localized in space and time. In one of the few papers based on the work of Zimin that has been translated into English, Aristov and Frick (1988, 1989) present a study of convection in a rotating fluid.

Like previous hot topics in science, the WT shows much promise but solid results have been difficult to achieve. The works of Meneveau (1991) and Zimin (1981) are far from final results; several more years are probably needed for those subjects to mature. However, for applications such as described in section 3 of this article, the WT is sufficiently developed that it can now be used with confidence as a tool in the oceanic and atmospheric sciences.

Acknowledgments. SDM is supported by the ONR Distinguished Educator Postdoctoral Fellowship to Dr. James O'Brien. The theoretical work of the Mesoscale Air–Sea Interaction Group is currently being supported by the Physical Oceanography Branch of the Office of Naval Research and the Ocean Processes Branch of NASA. Discussions on wavelet analysis with Dr. Bernard Barnier were useful. The color plates were created using the Ferret package, provided by Dr. D. E. Harrison and Steven Hankin. Thanks also to Mark Verschell for his on-site help with the Ferret routines.

APPENDIX

Wavelet Scales and Fourier Wavelengths

The relation between wavelet scale and the more common Fourier wavelength is not necessarily straightforward. For example, some wavelets are highly irregular without any dominant periodic components. In those cases it is probably a meaningless exercise to find a relation between the two disparate measures of distance. However, in the case of the Morlet wavelet, which is a periodic function enveloped by a Gaussian, it seems more reasonable. Using

$$g(x) = e^{icx}e^{-x^2/2},$$

we take the transform of e^{ik_0x} using (5)

$$T_g(b, a) = a^{1/2}\int_{-\infty}^{\infty} dk e^{ibk}H(k)e^{-(ak-c)^2/2}\delta(k - k_0).$$

This implies

$$|T_g(b, a)|^2 = a|\hat{g}(ak_0)|^2,$$

which in this case becomes

$$|T_g(b, a)|^2 = ae^{-(ak_0-c)^2}. \tag{A1}$$

To find the scale a of maximum correlation, we set the derivative of (A1) with respect to a equal to zero and obtain

$$1 + 2ck_0a - 2k_0^2a^2 = 0. \tag{A2}$$

Two solutions arise but only one is realistic. The preferred solution is

$$a_0 = \frac{1}{2}\left[\frac{c}{k_0} + \frac{(2 + c^2)^{1/2}}{k_0}\right]$$

Using $k_0 = 2\pi\lambda_0^{-1}$, the solution becomes a linear relation between wavelet scale and Fourier wavelength,

$$a_0 = \left[\frac{c + (2 + c^2)^{1/2}}{4\pi}\right]\lambda_0. \tag{A3}$$

The other solution is a decreasing function of λ_0 and is disregarded. Equation (A1) can also be obtained for a real monochromatic signal with any progressive wavelet.

Note, it follows from (2) that any linear superposition of periodic modes will result in separate local maxima, each described as above. The WT of any function

$$f(x) = \sum_j A_j e^{ik_jx} \tag{A4}$$

will have modulus maxima at $a_j = [c + (2 + c^2)^{1/2}] \times (2k_j)^{-1}$.

REFERENCES

Aristov, S. N. and P. G. Frick, 1988: Large-scale turbulence in a thin layer of nonisothermal rotating fluid. *Fluid Dyn.*, **23**, 522–528.

——, and ——, 1989: Large-scale turbulence in Rayleigh–Bernard convection. *Fluid Dyn.*, **24**, 43–48.

Combes, J. M., A. Grossman, and P. Tchamitchian, 1989: *Wavelets: Time Frequency Methods and Phase Space.* Springer, 315 pp.

Coulibaly, M. 1992: Analyse par ondolettes: Quelques aspects numeriques et applications a des signaux oceaniques simules et a l'estimation de densite de probabilite. Ph.D. thesis. L'universite Joseph Fourier-Grenoble, 209 pp.

Cox, M. D., 1980: Generation and propagation of 30-day waves in a numerical model of the Pacific. *J. Phys. Oceanogr.*, **10**, 217–248.

Duing, W., P. Hisard, E. Katz, J. Knauss, J. Meincke, L. Miller, K. Moroshkin, G. Philander, A. Rybnokov, K. Voigt, and R. Weisberg, 1975: Meanders and long waves in the equatorial Atlantic. *Nature*, **257**, 280–284.

Farge, M., 1992: Wavelet transforms and their applications to turbulence. *Ann. Rev. Fluid Mech.*, **24**, 395–457.

Gabor, D., 1946: Theory of communications. *J. Inst. Electr. Eng.*, **92**, 429–457.

Grossman, A., and J. Morlet, 1984: Decomposition of Hardy functions into square integrable wavelets of constant shape. *SIAM J. Math Anal.*, **15**, 723–736.

Kelly, B. G., 1992: On the generation and dispersion of Yanai waves with a spectral Chebyshev-collocation reduced-gravity ocean model. Ph.D. thesis. The Florida State University, 115 pp.

Kindle, J. C., and D. Thompson, 1989: The 26-day and 50-day os-

cilations in the western Indian Ocean: Model results. *J. Geophys. Res.*, **94C**, 4721–4736.

Legeckis, R., 1977: Long waves in the eastern equatorial Pacific Ocean: A view from a geostationary satellite. *Science*, **197**, 1179–1181.

Meneveau, C., 1991: Analysis of turbulence in the orthonormal wavelet representation. *J. Fluid Mech.*, **232**, 469–520.

Meyer, Y., 1985: Principe d'incertitude, bases hilbertiennes et algebres d'operateurs. *Seminaire Bourbaki, Asterisque*, Societe Mathematique de France, Paris, France, 662–684.

Moore, D. W., and S. G. H. Philander, 1977: Modeling of the tropical oceanic circulation. *The Sea*. Goldberg, E. D., I. N. McCrave, J. J. O'Brien and J. H. Steele, Eds. John Wiley & Sons, 319–361.

——, and J. P. McCreary, 1990: Excitation of intermediate-frequency equatorial waves at a western ocean boundary: With application to the Indian Ocean. *J. Geophy. Res.*, **95C**, 5219–5231.

Morlet, J., 1983: Sampling theory and wave propagation. *NATO ASI Series, 1. Issues in Acoustic Signal/Image Processing and Recognition*. Chen, C. H., Ed. Springer, 233–261.

Murenzi, R., 1989: Wavelet transforms associated to the N-dimensional Euclidean group with dilations: signal in more than one dimension. *Wavelets: Time Frequency Methods and Phase Space*, Combes, J. M., A. Grossman and P. Tchamitchian, Eds. Springer, 239–246.

Philander, S. G. H., 1976: Instabilities of zonal equatorial currents. *J. Geophy. Res.*, **81**, 3725–3735.

——, 1978: Instabilities of zonal equatorial currents 2. *J. Geophy. Res.*, **83**, 3679–3682.

Ruskai, M. B., G. Beylkin, R. Coifman, I. Daubechies, S. Mallat, Y. Meyer, and L. Raphael, 1992: *Wavelets and their Applications*. Jones and Barlett Publishers, 474 pp.

Tsai, P. T. H., 1990: The 26-day oscillation in the satellite SST measurements in the equatorial western Indian Ocean. M.S. thesis, The Florida State University, Department of Meteorology, 1–50.

Weisberg, R. H., and T. J. Weingartner, 1979: Instability waves in the equatorial Atlantic Ocean. *J. Geophy. Res.*, **94c**, 17 985–18 002.

Weisberg, R. H., and A. M. Horigan, 1981: Low frequency variability in the equatorial Atlantic. *J. Phys. Oceanogr.*, **11**, 913–920.

Weisberg, R. H., A. M. Horigan, and C. Colin, 1979: Equatorially trapped Rossby–gravity propagation in the Gulf of Guinea. *J. Mar. Res.*, **37**, 67–86.

Woodberry, K. E., M. E. Luther, and J. J. O'Brien, 1989: The wind-driven seasonal circulation in the southern tropical Indian Ocean. *J. Geophy. Res.*, **94C**, 17 985–18 002.

Zimlin, V. D. 1981: Hierarchical model of turbulence. *Izv. Atmos. Ocean. Phys.*, **17**, 941–949.